IEEE Robotics and Automation Letters (RAL) paper presented at
2024 IEEE/RSJ International Conference on Intelligent Robots and Systems (IROS)
October 14-18, 2024. Abu Dhabi, UAE

Simple-Rotation Angle/Axis Representations Based Second-Order Impedance Control

Chenwei Gong, Fei Zhao, *Member, IEEE*, Zhiwei Liao, Tao Tao, Xiao Wang, and Xuesong Mei

***Abstract*—Since the difference in angular velocity is used as the derivative of the orientation error in the classical impedance control, there is no longer a form of the second-order differential equation (SODE), and there is non-linearity in the classical impedance control, which limits applications. To address this problem, this article uses simple-rotation angle/axis representations (SRAAR), as well as their derivatives, to describe the end-effector's orientation displacement and its derivatives in impedance control. As a result, an SRAAR-based second-order impedance control, whose dynamic relationship has the form of SODE, is proposed. Furthermore, as a direct application of the proposed SRAAR-based second-order impedance control, an adaptive control method is also proposed to deal with the problem of uncertain dynamic parameters so that the desired dynamic relationship can be accurately realized. A simulation is carried out to show the difference between the classical impedance control and the proposed impedance control. Experiments on the Franka Emika Panda have been conducted, and the results validate the effectiveness of the proposed adaptive control, which also verifies the correctness of the proposed SRAAR-based second-order impedance control.**

***Index Terms*—Impedance control, simple-rotation angle/axis representations (SRAAR), second-order differential equation (SODE), adaptive control.**

I. Introduction

IMPEDANCE control tries to achieve a desired dynamic relationship, called the impedance model in this article, between the encountered force coming from the environment and the movement of the robot end-effector. It has been proven to be an advisable control framework for contact-rich scenarios and has been widely adopted [1].

In impedance control, the robot end-effector's displacement can be divided into two parts, i.e., position displacement and orientation displacement. It is well known that the position displacement is obtained by directly subtracting the desired Cartesian position from the actual Cartesian position of the robot end-effector, as a kind of vector subtraction. Unlike position displacement, there are several orientation displacement representations such as quaternion [2], Euler angles [3], and angle/axis representations [4]. Angle/axis representations can be further classified [4], i.e., Euler parameters, classical angle/axis, Rodrigues parameters, and simple-rotation. Quaternion is the same as the Euler parameters of angle/axis representations when used in impedance control [2]. Euler angles are one of the most classical orientation representations. However, since Euler angles should follow a certain rotational sequence, they might cause directional inconsistencies between the external torque and the end-effector rotation in impedance control [5]. Additionally, there is a singularity problem for Euler angles [3]. Angle/axis representations are composed of a scalar function and a unit vector. For Euler parameters and classical angle/axis, although they do not exhibit the aforementioned defects of Euler angles [2], since a sine function is used, the norm of orientation displacement must not be greater than 1, which implicitly restricts the range of external torque [6]. For Rodrigues parameters, a tangent function is used, which means there is no limitation for external torque. However, a singularity exists for 180° rotations [7]. Simple-rotation parameters are composed of the product of the rotation angle and the rotation axis. Compared with the other aforementioned representations, simple-rotation parameters have properties such as being singularity-free, ensuring directional consistency between rotation and external torque, and having no limitations on external torque simultaneously.

Usually, the impedance model is required to have a form of a second-order differential equation (SODE) [8]. However, the impedance model commonly used is the same as the one proposed by [4], wherein some imperfections exist, as demonstrated below. If we divide the impedance model into two decoupling parts roughly, i.e., position-force relationship and rotation-torque relationship, the position-force relationship generally has the form of SODE, whereas no such characteristic exists for the rotation-torque part in [4]. This is because the angular velocity difference and the angular acceleration difference are used as the high-order terms of orientation displacement. This defect may lead to additional challenges; for example, in [9], a special Lyapunov function is needed to prove the stability of the given impedance model. Sometimes, such a defect is ignored in the proof, leading to discrepancies between the proof and the actual application [10].

On the other hand, most current works on impedance control only focus on the position-force part, with few paying attention to the rotation-torque part. In [11], impedance control with adaptation is achieved, where a dynamic parameter adaptation algorithm is proposed to tackle the problem of dynamic parameter uncertainty and to realize the desired impedance model

Manuscript received 15 December 2023; accepted 12 April 2024. Date of publication 1 May 2024; date of current version 13 May 2024. This letter was recommended for publication by Associate Editor P. Di Lillo and Editor C. Gosselin upon evaluation of the reviewers' comments. This work was supported by the National Natural Science Foundation of China under Grant 52175029. *(Corresponding author: Fei Zhao.)*

The authors are with the State Key Laboratory for Manufacturing System Engineering, Xi'an Jiaotong University, Xi'an, Shaanxi 710049, China, and also with the Shaanxi Key Laboratory of Intelligent Robots and School of Mechanical Engineering, Xi'an Jiaotong University, Xi'an, Shaanxi 710049, China (e-mail: og12138@stu.xjtu.edu.cn; ztzhao@mail.xjtu.edu.cn; liao.zhiwei@stu.xjtu.edu.cn; taotao@mail.xjtu.edu.cn; wangxiao2020@stu.xjtu.edu.cn; xsmei@mail.xjtu.edu.cn).

This letter has supplementary downloadable material available at https://doi.org/10.1109/LRA.2024.3396090, provided by the authors.

Digital Object Identifier 10.1109/LRA.2024.3396090

accurately. In [12], the desired position in impedance control is adjusted adaptively to help the robot track the desired contact force under environmental uncertainty. A similar algorithm is given in [13], and impedance parameters are adjusted adaptively to track the desired contact force. In [14], the stability of the impedance model with variable impedance parameters is considered, and a mathematical relationship between impedance parameters is provided to ensure stable behavior. All of these studies are based on a second-order impedance model, or only force and linear motion are considered in these studies, regardless of external torque or angular motion. The aforementioned works might be extended to the rotation-torque part if the rotation-torque relationship also has the form of SODE. Additionally, the well-studied linear system theory can be exploited. An obvious example is that the method proposed in [11] can be extended to the rotation-torque part, and the whole impedance model including the rotation-torque part can be realized accurately. Another example is that the result derived in [14] can be used directly by replacing the joint variables with the end-effector's displacement.

In summary, an impedance control using simple-rotation angle/axis representations (SRAAR) with the form of SODE is needed. To the best of our knowledge, there has still been no work considering this type of impedance control. To achieve this type of impedance control, referring to the implementation of the classical impedance control, the value of SRAAR and its first-order derivative should be known, and the first-order and the second-order differential relationships between SRAAR and joint angles are also needed. In [15], a differential relationship between angular velocity and the first-order derivative of SRAAR is proposed. This relationship could be used to realize the second-order impedance control. However, the more essential relationships, i.e., the relationships between the derivative of rotation angle, the derivative of rotation axis, and angular velocity, are not provided in that article. These essential relationships are obtained in [16] through the quaternion propagation rule. Nevertheless, both of the above methods will fail when the rotation angle is zero, which is still unsolved.

Faced with the aforementioned challenges, this letter proposes an SRAAR-based second-order impedance control, and the main contributions are summarized as follows:

1) A novel method is proposed to calculate the first-order derivative of SRAAR, where two auxiliary variables are employed to simplify the calculation. The complete first-order and second-order differential relationships between SRAAR and joint angles are also proposed.
2) Subsequently, a type of SRAAR-based second-order impedance control is realized.
3) Furthermore, an adaptive impedance control is proposed as a direct application of the proposed SRAAR-based second-order impedance control to realize the entire impedance model accurately.

The letter is organized as follows. Section II introduces the robot model and the classical impedance control. In Section III, the methods to calculate the zero-order and first-order derivatives of SRAAR are provided in subsections III-A and III-B. The first-order and second-order differential relationships between SRAAR and joint angles are presented in subsection III-C. A method to implement the proposed SRAAR-based second-order impedance control using an open-loop approach is discussed in subsection III-D. Additionally, an adaptive control is presented in subsection III-E. In Section IV, a simulation is carried out to demonstrate the difference between the classical impedance control and the proposed impedance control. In Section V, experiments with a 7-DOF manipulator verify the proposed approach. Finally, conclusions are drawn in Section VI.

II. Background

A. Robot Model

The dynamics of an n-DOF rigid manipulator in joint space can be written as [3]:

$$\boldsymbol{B}(\boldsymbol{q})\ddot{\boldsymbol{q}} + \boldsymbol{C}(\boldsymbol{q},\dot{\boldsymbol{q}})\dot{\boldsymbol{q}} + \boldsymbol{G}(\boldsymbol{q}) + \boldsymbol{\tau}_f = \boldsymbol{\tau} + \boldsymbol{J}(\boldsymbol{q})^T\boldsymbol{F}_e \tag{1}$$

where $\boldsymbol{q} \in R^{n\times 1}$ denotes the joint displacement of the robot, and $\dot{\boldsymbol{q}}, \ddot{\boldsymbol{q}} \in R^{n\times 1}$ represent the joint velocity and acceleration, respectively; $\boldsymbol{B}(\boldsymbol{q}) \in R^{n\times n}$ is the inertia matrix; $\boldsymbol{C}(\boldsymbol{q},\dot{\boldsymbol{q}}) \in R^{n\times n}$ is the Coriolis and centrifugal force matrix; $\boldsymbol{G}(\boldsymbol{q}) \in R^{n\times 1}$ is the gravitational term; $\boldsymbol{\tau}_f \in R^{n\times 1}$ is the joint friction torque; $\boldsymbol{\tau} \in R^{n\times 1}$ is the command torque; $\boldsymbol{J}(\boldsymbol{q}) \in R^{6\times n}$ is the geometrical Jacobian of the robot end-effector; $\boldsymbol{F}_e \in R^{6\times 1}$ is the environment effort applied to the robot end-effector, and $\boldsymbol{F}_e$ can be written as $\left[\boldsymbol{f}_e^T, \boldsymbol{\tau}_e^T\right]^T$, where $\boldsymbol{f}_e \in R^{3\times 1}$ and $\boldsymbol{\tau}_e \in R^{3\times 1}$ are the actual environment force and torque.

Use $\boldsymbol{p} \in R^{3\times 1}$ and $\boldsymbol{R} \in SO(3)$ to represent the Cartesian position and the rotation matrix of the robot end-effector under the base frame, respectively. Then there are mathematical relationships: $\dot{\boldsymbol{p}} = \boldsymbol{J}_p\dot{\boldsymbol{q}}$ and $\dot{\boldsymbol{R}} = \hat{\boldsymbol{\omega}}\boldsymbol{R} = \widehat{\boldsymbol{J}_o\dot{\boldsymbol{q}}}\boldsymbol{R}$, where $\boldsymbol{\omega} \in R^{3\times 1}$ is the angular velocity of the end-effector; $\boldsymbol{J}_p, \boldsymbol{J}_o \in R^{3\times n}$ are the matrices relating the contribution of the joint velocities to the end-effector linear velocity and angular velocity, respectively. And there is $\boldsymbol{J} = \left[\boldsymbol{J}_p^T, \boldsymbol{J}_o^T\right]^T$. $\hat{*}$ is an antisymmetric operator, and the cross product of two 3D vectors, i.e., $\boldsymbol{a} \times \boldsymbol{b}$, equals to $\hat{\boldsymbol{a}}\boldsymbol{b}$.

The dynamic model of an n-DOF rigid manipulator can be formulated with a linear form [17], i.e.,

$$\boldsymbol{B}(\boldsymbol{q})\ddot{\boldsymbol{q}} + \boldsymbol{C}(\boldsymbol{q},\dot{\boldsymbol{q}})\dot{\boldsymbol{q}} + \boldsymbol{G}(\boldsymbol{q}) = \boldsymbol{Y}(\boldsymbol{q},\dot{\boldsymbol{q}},\ddot{\boldsymbol{q}})\phi \tag{2}$$

where $\boldsymbol{Y} \in R^{n\times 11n}$ is the linear regressor matrix; $\boldsymbol{\phi} \in R^{11n\times 1}$, which is seen as a constant vector, is the dynamic parameters of the robot.

B. Classical Impedance Control

Classical impedance model is formulated typically as:

$$\boldsymbol{M}\begin{bmatrix}\ddot{\boldsymbol{p}} - \ddot{\boldsymbol{p}}_d \\ \dot{\boldsymbol{\omega}} - \dot{\boldsymbol{\omega}}_d\end{bmatrix} + \boldsymbol{D}\begin{bmatrix}\dot{\boldsymbol{p}} - \dot{\boldsymbol{p}}_d \\ \boldsymbol{\omega} - \boldsymbol{\omega}_d\end{bmatrix} + \boldsymbol{K}\begin{bmatrix}\boldsymbol{p} - \boldsymbol{p}_d \\ \boldsymbol{\varphi}\end{bmatrix} = \begin{bmatrix}\boldsymbol{f}_e - \boldsymbol{f}_d \\ \boldsymbol{\tau}_e - \boldsymbol{\tau}_d\end{bmatrix} \tag{3}$$

where $\boldsymbol{M}, \boldsymbol{D}, \boldsymbol{K} \in R^{6\times 6}$ are the desired inertia, damping, and stiffness matrices; $\boldsymbol{p}_d$, $\boldsymbol{\omega}_d \in R^{3\times 1}$ are the desired Cartesian position and the desired angular velocity of the end-effector; $\boldsymbol{f}_d$, $\boldsymbol{\tau}_d \in R^{3\times 1}$ are the desired environment force and torque; $\boldsymbol{\varphi} \in R^{3\times 1}$ is the orientation displacement between the desired and the actual frames of the end-effector. $\boldsymbol{\varphi}$ could be Euler angles or angle/axis representations or others as mentioned in Section I. The value of $\boldsymbol{\varphi}$ depends on the type of $\boldsymbol{\varphi}$.

The angular velocity difference and the angular acceleration difference in (3) are introduced by the following method. In [4], a generalized rotational kinetic energy is defined as a quadratic function of the angular velocity difference. By utilizing the

derivative of energy equaling the dot product of torque and angular velocity, the angular acceleration difference is introduced into the impedance model. The weight in the generalized rotational kinetic energy, i.e., the coefficient of the angular acceleration difference in the impedance model, can be regarded as the moment of inertia. Similarly, a damping term, which is the product of a damping matrix and the angular velocity difference, is also introduced.

The stability of (3) is proven as follows. In [4], when $\boldsymbol{\varphi}$ is represented using angle/axis representations, a rotation potential energy is also defined. The rotational stiffness is determined by this energy, such that the time derivative of the total rotation energy is a quadratic function of the angular velocity error. Consequently, the angular velocity error converges to zero; the stability is proven. In [9], when $\boldsymbol{\varphi}$ is represented using quaternion, the Lyapunov function is composed of a translational potential energy function, a rotation potential energy function, and a quadratic function of the angular velocity error weighted by $\boldsymbol{K}$. Subsequently, the time derivative of the Lyapunov function is a quadratic function of the angular velocity error weighted by $\boldsymbol{D}$, and the stability of (3) is proven finally.

III. SRAAR-Based Second-Order Impedance Control

As mentioned in Section I, an impedance control using SRAAR with the form of SODE is needed. Consequently, the desired impedance model can be represented as

$$\boldsymbol{M}\begin{bmatrix}\ddot{\boldsymbol{p}}-\ddot{\boldsymbol{p}}_d\\ (\ddot{\theta\boldsymbol{l}})\end{bmatrix}+\boldsymbol{D}\begin{bmatrix}\dot{\boldsymbol{p}}-\dot{\boldsymbol{p}}_d\\ (\dot{\theta\boldsymbol{l}})\end{bmatrix}+\boldsymbol{K}\begin{bmatrix}\boldsymbol{p}-\boldsymbol{p}_d\\ \theta\boldsymbol{l}\end{bmatrix}=\begin{bmatrix}\boldsymbol{f}_e-\boldsymbol{f}_d\\ \boldsymbol{\tau}_e-\boldsymbol{\tau}_d\end{bmatrix} \tag{4}$$

where $\theta\boldsymbol{l}$ is the SRAAR between the desired rotation matrix $\boldsymbol{R}_d\in SO(3)$ and the actual rotation matrix $\boldsymbol{R}$ of the end-effector; $\boldsymbol{l}\in R^{3\times1}$ is a unit vector and is expressed in the base frame; θ is a scalar. And $\theta\boldsymbol{l}$ satisfies

$$\widetilde{\boldsymbol{R}}=\boldsymbol{R}\boldsymbol{R}_d^T=e^{\theta\boldsymbol{l}}=\cos(\theta)\boldsymbol{I}+\sin(\theta)\hat{\boldsymbol{l}}+(1-\cos(\theta))\boldsymbol{l}\boldsymbol{l}^T \tag{5}$$

The physical meaning of $\theta\boldsymbol{l}$ is that $\boldsymbol{R}$ can be obtained by rotating $\boldsymbol{R}_d$ by θrad along the vector $\boldsymbol{l}$; θ and $\boldsymbol{l}$ could be seen as the rotation angle and the rotation axis, respectively.

If $\theta\boldsymbol{l}$ is regarded as the rotating axis vector with length θ between $\boldsymbol{R}_d$ and $\boldsymbol{R}$, (4) demonstrates how torque influences changes in the size and orientation of the rotation axis $\theta\boldsymbol{l}$. Furthermore, in Euclidean space, a vector can be regarded as a point, and $(\dot{\theta\boldsymbol{l}})$ and $(\ddot{\theta\boldsymbol{l}})$ can be considered as the velocity and the acceleration of the point; $\boldsymbol{M}$ and $\boldsymbol{D}$ contain inertia and damping information of the point. Alternatively, $\theta\boldsymbol{l}$ can be viewed as the geodesic between $\boldsymbol{R}_d$ and $\boldsymbol{R}$, and (4) illustrates how this geodesic changes. Additionally, from the perspective of Lie groups and Lie algebras, $\theta\boldsymbol{l}$ lies in the tangent space at the identity and can be seen as an element of the Lie algebras, and (4) illustrates how the element changes in the tangent space.

To implement the proposed impedance model (4), the key is to determine the value of $\theta\boldsymbol{l}$, obtain the value of $(\dot{\theta\boldsymbol{l}})$, and establish the relationship between $(\ddot{\theta\boldsymbol{l}})$ and $\ddot{\boldsymbol{q}}$.

A. Value of $\theta\boldsymbol{l}$

According to (5), θ can always be calculated by $\theta=arccos((tr(\widetilde{\boldsymbol{R}})-1)/2)$.

When θ is not 0 or π, $\boldsymbol{l}$ can be calculated by $\boldsymbol{l}=(\widetilde{\boldsymbol{R}}-\widetilde{\boldsymbol{R}}^T)^\vee/2/\sin(\theta)$, where $(*)^\vee$ represents the reverse operation of $\hat{*}$. In this situation, the value of $\theta\boldsymbol{l}$ is obtained by θ multiplying $\boldsymbol{l}$.

When θ is π, the absolute value of the i-th component of $\boldsymbol{l}$ is $\sqrt{(\widetilde{\boldsymbol{R}}_{ii}+1)/2}$. Consequently, $\boldsymbol{l}$ can be obtained by attempting to change the sign of each component. In this situation, the value of $\theta\boldsymbol{l}$ is also obtained by θ multiplying $\boldsymbol{l}$.

When θ is 0 and only $\widetilde{\boldsymbol{R}}$ is available, although $\boldsymbol{l}$ is incalculable, there is still $\theta\boldsymbol{l}=\boldsymbol{0}$.

To sum up, $\theta\boldsymbol{l}$ and θ are always calculable, and $\boldsymbol{l}$ is calculable when $\theta\neq0$.

B. Value of $(\dot{\theta\boldsymbol{l}})$

After differentiating both sides of (5), it has

$$\begin{aligned}\dot{\widetilde{\boldsymbol{R}}}=&(-s_\theta\boldsymbol{I}+c_\theta\hat{\boldsymbol{l}}+s_\theta\boldsymbol{l}\boldsymbol{l}^T)\dot{\theta}\\&+s_\theta\dot{\hat{\boldsymbol{l}}}+(1-c_\theta)(\dot{\boldsymbol{l}}\boldsymbol{l}^T+\boldsymbol{l}\dot{\boldsymbol{l}}^T)\end{aligned} \tag{6}$$

where s_θ denotes $\sin(\theta)$ and c_θ is $cos(\theta)$. The value of $(\dot{\theta\boldsymbol{l}})$ is discussed in the following situations:

1) When $\theta\neq0,\pm\pi/2$: First, derive the expression of $\dot{\boldsymbol{l}}$. Since θ is not 0, $\boldsymbol{l}$ can be calculated as said in III-A. Transpose the result obtained by left-multiplying $\boldsymbol{l}^T$ by $\dot{\widetilde{\boldsymbol{R}}}$, and add the result obtained by right-multiplying $\boldsymbol{l}$ by $\dot{\widetilde{\boldsymbol{R}}}$, i.e., $(\boldsymbol{l}^T\dot{\widetilde{\boldsymbol{R}}})^T+\dot{\widetilde{\boldsymbol{R}}}\boldsymbol{l}$. Using $\dot{\boldsymbol{l}}^T\boldsymbol{l}=\boldsymbol{l}^T\dot{\boldsymbol{l}}=0$, it has

$$\dot{\boldsymbol{l}}=\frac{(\dot{\widetilde{\boldsymbol{R}}}+\dot{\widetilde{\boldsymbol{R}}}^T)\boldsymbol{l}}{2(1-c_\theta)} \tag{7}$$

Then, derive the expression of $\dot{\theta}$. For the calculated unit vector $\boldsymbol{l}$, it can always find two unit vectors $\boldsymbol{\alpha}$ and $\boldsymbol{\beta}$ satisfying $\boldsymbol{\alpha}\times\boldsymbol{l}=\boldsymbol{\beta}$. Multiply $\boldsymbol{\alpha}^T$ left by $\dot{\widetilde{\boldsymbol{R}}}$, and multiply $\boldsymbol{\beta}$ right, and utilize $\boldsymbol{\alpha}^T\hat{\boldsymbol{l}}\boldsymbol{\beta}=0$; it yields

$$\dot{\theta}=\frac{\boldsymbol{\alpha}^T\dot{\widetilde{\boldsymbol{R}}}\boldsymbol{\beta}}{c_\theta} \tag{8}$$

After getting the value of $\dot{\boldsymbol{l}}$ and $\dot{\theta}$, $(\dot{\theta\boldsymbol{l}})$ is just $\dot{\theta}\boldsymbol{l}+\theta\dot{\boldsymbol{l}}$.

2) When $\theta\neq0,\pi$: For $\dot{\boldsymbol{l}}$, because $\theta\neq0$, the above derivation of $\dot{\boldsymbol{l}}$ also holds, i.e., (7) also holds.

For $\dot{\theta}$, similar to (8), multiply $\boldsymbol{\alpha}^T$ left by $\dot{\widetilde{\boldsymbol{R}}}$, and multiply $\boldsymbol{\alpha}$ right; it has

$$\dot{\theta}=-\frac{\boldsymbol{\alpha}^T\dot{\widetilde{\boldsymbol{R}}}\boldsymbol{\alpha}}{s_\theta} \tag{9}$$

In this situation, $(\dot{\theta\boldsymbol{l}})$ can also be obtained by $\dot{\theta}\boldsymbol{l}+\theta\dot{\boldsymbol{l}}$.

3) When $\theta=0$: (6) reduces to $\dot{\widetilde{\boldsymbol{R}}}=\dot{\theta}\hat{\boldsymbol{l}}$. Thus, it has $(\dot{\theta\boldsymbol{l}})=(\dot{\widetilde{\boldsymbol{R}}})^\vee$.

To sum up, the value of $(\dot{\theta\boldsymbol{l}})$ is always calculable.

C. Relationship Between $(\ddot{\theta}\boldsymbol{l})$ and $\ddot{\boldsymbol{q}}$

1) When $\theta \neq 0, \pm\pi/2$: Using (7) and (8), $(\dot{\theta}\boldsymbol{l})$ can be calculated as

$$(\dot{\theta}\boldsymbol{l}) = \theta\dot{\boldsymbol{l}} + \boldsymbol{l}\dot{\theta} = \frac{\theta(\dot{\tilde{\boldsymbol{R}}} + \dot{\tilde{\boldsymbol{R}}}^T)\boldsymbol{l}}{2(1-c_\theta)} + \frac{\boldsymbol{l}\boldsymbol{\alpha}^T\dot{\tilde{\boldsymbol{R}}}\boldsymbol{\beta}}{c_\theta} \tag{10}$$

Reshaping the above equation utilizing $\dot{\boldsymbol{R}} = \hat{\boldsymbol{\omega}}\boldsymbol{R} = \widehat{\boldsymbol{J}_o\dot{\boldsymbol{q}}}\boldsymbol{R}$ and $\hat{\boldsymbol{a}}\boldsymbol{b} = -\hat{\boldsymbol{b}}\boldsymbol{a}$, it has

$$(\dot{\theta}\boldsymbol{l}) = \boldsymbol{J}_{o_1'}\dot{\boldsymbol{q}} + \boldsymbol{\gamma}_1 \tag{11}$$

where

$$\boldsymbol{J}_{o_1'} = \frac{\theta(\boldsymbol{R}_d\boldsymbol{R}^T\hat{\boldsymbol{l}} - \widehat{\boldsymbol{R}\boldsymbol{R}_d^T\boldsymbol{l}})\boldsymbol{J}_o}{2(1-c_\theta)} - \frac{\boldsymbol{l}\boldsymbol{\alpha}^T}{c_\theta}\widehat{\boldsymbol{R}\boldsymbol{R}_d^T}\boldsymbol{\beta}\boldsymbol{J}_o \tag{12}$$

$$\boldsymbol{\gamma}_1 = \frac{\theta(\boldsymbol{R}\dot{\boldsymbol{R}}_d^T + \dot{\boldsymbol{R}}_d\boldsymbol{R}^T)\boldsymbol{l}}{2(1-c_\theta)} + \frac{\boldsymbol{l}\boldsymbol{\alpha}^T}{c_\theta}\boldsymbol{R}\dot{\boldsymbol{R}}_d^T\boldsymbol{\beta} \tag{13}$$

To establish the relationship between $(\ddot{\theta}\boldsymbol{l})$ and $\ddot{\boldsymbol{q}}$, a natural approach is to differentiate both sides of (11). However, differentiation necessitates the function to be continuously differentiable. Differentiating $\boldsymbol{J}_{o_1'}$ and $\boldsymbol{\gamma}_1$ requires $\boldsymbol{\alpha}$ and $\boldsymbol{\beta}$ to be continuously differentiable with respect to time, which implies additional planning for $\boldsymbol{\alpha}$ and $\boldsymbol{\beta}$ is necessary, resulting in additional challenges. The following lemma addresses this issue.

Lemma 3.1: When $\theta \neq 0, \pm\pi/2$, it has

$$(\ddot{\theta}\boldsymbol{l}) = \boldsymbol{J}_{o_1'}\ddot{\boldsymbol{q}} + \boldsymbol{\Gamma}_1 \tag{14}$$

where $\boldsymbol{\Gamma}_1 = \dot{\boldsymbol{J}}_{o_1'}\dot{\boldsymbol{q}} + \dot{\boldsymbol{\gamma}}_1$, and $\boldsymbol{J}_{o_1'}$ is calculated by (12), and $\dot{\boldsymbol{J}}_{o_1'}$ and $\dot{\boldsymbol{\gamma}}_1$ have the same expressions as the results obtained by deriving (12) and (13) under the situation where $\boldsymbol{\alpha}$ and $\boldsymbol{\beta}$ are continuously differentiable. But now, in $\dot{\boldsymbol{J}}_{o_1'}$ and $\dot{\boldsymbol{\gamma}}_1$, $\boldsymbol{\alpha}$, $\boldsymbol{\beta}$, $\dot{\boldsymbol{\alpha}}$, and $\dot{\boldsymbol{\beta}}$ can be chosen arbitrarily as long as they satisfy that

1. $\boldsymbol{\alpha} \times \boldsymbol{l} = \boldsymbol{\beta}$.
2. it has $[\dot{\boldsymbol{\alpha}}, \dot{\boldsymbol{l}}, \dot{\boldsymbol{\beta}}] = \hat{\boldsymbol{\omega}}_l[\boldsymbol{\alpha}, \boldsymbol{l}, \boldsymbol{\beta}]$, for some $\boldsymbol{\omega}_l \in R^{3\times 1}$.

Proof: If $\boldsymbol{R}_d(t)$ is given, for any given $\boldsymbol{R}(t)$, there must be a unique $\dot{\theta}(t)$ and $\ddot{\theta}(t)$ corresponding to the given $\boldsymbol{R}(t)$. Thus, for any continuously derivable unit vector $\boldsymbol{\alpha}'(t)$ and $\boldsymbol{\beta}'(t)$ that satisfy $\boldsymbol{\alpha}'(t) \times \boldsymbol{l}(t) \equiv \boldsymbol{\beta}'(t)$, (8) and differentiating (8) yield the same $\dot{\theta}(t)$ and $\ddot{\theta}(t)$. Besides, at a certain moment t_0, if we arbitrarily choose $\boldsymbol{\alpha}_0$, $\boldsymbol{\beta}_0$, $\dot{\boldsymbol{\alpha}}_0$, and $\dot{\boldsymbol{\beta}}_0$ satisfying the above two conditions, there will always exist a set of $\boldsymbol{\alpha}'(t)$ and $\boldsymbol{\beta}'(t)$ whose values are $\boldsymbol{\alpha}_0$, $\boldsymbol{\beta}_0$ and whose derivatives are $\dot{\boldsymbol{\alpha}}_0$ and $\dot{\boldsymbol{\beta}}_0$ at this moment. And then, bring the founded $\boldsymbol{\alpha}'(t)$ and $\boldsymbol{\beta}'(t)$ into (8), and differentiate both sides of (8) at t_0. Because $\dot{\theta}(t)$ and $\ddot{\theta}(t)$ are the same for all $\boldsymbol{\alpha}'(t)$ and $\boldsymbol{\beta}'(t)$, as mentioned before, using $\dot{\boldsymbol{R}} = \hat{\boldsymbol{\omega}}\boldsymbol{R} = \widehat{\boldsymbol{J}_o\dot{\boldsymbol{q}}}\boldsymbol{R}$ and $\hat{\boldsymbol{a}}\boldsymbol{b} = -\hat{\boldsymbol{b}}\boldsymbol{a}$, Lemma 3.1 can be proven.

2) When $\theta \neq 0, \pi$: Using (7) and (9), and following the steps before, it's easy to establish the relationships between $(\dot{\boldsymbol{l}}\boldsymbol{l})$ and $\dot{\boldsymbol{q}}$, and between $(\ddot{\theta}\boldsymbol{l})$ and $\ddot{\boldsymbol{q}}$, similar to (11) and (14).

3) When $\theta = 0$: According to the Appendix, two equations similar to (11) and (14) can also be derived.

To sum up, there are general equations

$$\begin{aligned}(\dot{\boldsymbol{l}}\boldsymbol{l}) &= \boldsymbol{J}_{o'}\dot{\boldsymbol{q}} + \boldsymbol{\gamma}\\ (\ddot{\boldsymbol{l}}\boldsymbol{l}) &= \boldsymbol{J}_{o'}\ddot{\boldsymbol{q}} + \boldsymbol{\Gamma}\end{aligned} \tag{15}$$

D. Second-Order Impedance Control

Then, the command torque of impedance control with the impedance model (4) can be calculated by referring to the calculation process of general impedance control. However, in reality, it's difficult to obtain accurate dynamic parameters, and only estimates are available. Thus, the command torque satisfies

$$\begin{aligned}\boldsymbol{M}\boldsymbol{J}'\bar{\boldsymbol{B}}^{-1}\boldsymbol{\tau} = &\begin{bmatrix}\boldsymbol{f}_e - \boldsymbol{f}_d\\ \boldsymbol{\tau}_e - \boldsymbol{\tau}_d\end{bmatrix} + \boldsymbol{M}\begin{bmatrix}\ddot{\boldsymbol{p}}_d - \dot{\boldsymbol{J}}_p\dot{\boldsymbol{q}}\\ -\boldsymbol{\Gamma}\end{bmatrix}\\ &- \boldsymbol{D}\begin{bmatrix}\dot{\boldsymbol{p}} - \dot{\boldsymbol{p}}_d\\ (\dot{\theta}\boldsymbol{l})\end{bmatrix} - \boldsymbol{K}\begin{bmatrix}\boldsymbol{p} - \boldsymbol{p}_d\\ \theta\boldsymbol{l}\end{bmatrix}\\ &+ \boldsymbol{M}\boldsymbol{J}'\bar{\boldsymbol{B}}^{-1}(\bar{\boldsymbol{C}}\dot{\boldsymbol{q}} + \bar{\boldsymbol{G}} + \bar{\boldsymbol{\tau}}_f - \boldsymbol{J}^T\boldsymbol{F}_e)\end{aligned} \tag{16}$$

where $\bar{\boldsymbol{B}}, \bar{\boldsymbol{C}} \in R^{n\times n}$, $\bar{\boldsymbol{G}} \in R^{n\times 1}$, and $\bar{\boldsymbol{\tau}}_f \in R^{n\times 1}$ are the estimated inertia, Coriolis and centrifugal force, gravitational and joint friction matrices respectively, and $\boldsymbol{J}' = [\boldsymbol{J}_p^T, \boldsymbol{J}_{o'}^T]^T$.

Since the term $\boldsymbol{J}^T\boldsymbol{F}_e$ is also introduced from the perspective of energy, i.e., the principle of virtual work, by using the so-called natural inertia, the classical impedance control can be achieved without external force measurement. However, since $\boldsymbol{J}'$ is used in the last term of (16), it seems that $\boldsymbol{F}_e$ cannot be eliminated when $\boldsymbol{M}$ is set to be a symmetric positive definite matrix. In other words, when $\boldsymbol{M}$ is set to be a symmetric positive definite matrix, external force measurement or estimation is still necessary.

E. Adaptive Second-Order Impedance Control

It's evident that it would not achieve the desired impedance model without accurate dynamic parameters. The work [11] deals with this problem, where two adaptive control methods are proposed. However, the first method in that article only considers the position-force part in impedance control and relies on a second-order impedance model. Since a second-order impedance model is developed in this article, our approach can be integrated with the method proposed in [11]. Consequently, the impedance model, including the rotation-torque part, can be realized accurately instead of just the position-force part, which shows the application possibility of the proposed second-order impedance model.

Bringing the command torque $\boldsymbol{\tau}$ calculated by (16) into the real dynamic model (1) and utilizing (2), there is

$$\begin{aligned}&\boldsymbol{M}\boldsymbol{J}'\bar{\boldsymbol{B}}^{-1}(\boldsymbol{\tau}_f - \bar{\boldsymbol{\tau}}_f - \boldsymbol{Y}\widetilde{\boldsymbol{\phi}}) + \boldsymbol{M}\begin{bmatrix}\ddot{\boldsymbol{p}} - \ddot{\boldsymbol{p}}_d\\ (\ddot{\theta}\boldsymbol{l})\end{bmatrix}\\ &+ \boldsymbol{D}\begin{bmatrix}\dot{\boldsymbol{p}} - \dot{\boldsymbol{p}}_d\\ (\dot{\theta}\boldsymbol{l})\end{bmatrix} + \boldsymbol{K}\begin{bmatrix}\boldsymbol{p} - \boldsymbol{p}_d\\ \theta\boldsymbol{l}\end{bmatrix} = \begin{bmatrix}\boldsymbol{f}_e - \boldsymbol{f}_d\\ \boldsymbol{\tau}_e - \boldsymbol{\tau}_d\end{bmatrix}\end{aligned} \tag{17}$$

where $\widetilde{\boldsymbol{\phi}} = \bar{\boldsymbol{\phi}} - \boldsymbol{\phi}$ and $\bar{\boldsymbol{\phi}} \in R^{11n\times 1}$ is an estimation of $\boldsymbol{\phi}$. Furthermore, suppose the friction is modeled as $\boldsymbol{\tau}_f = diag(\boldsymbol{k}_v)\dot{\boldsymbol{q}} + diag(\boldsymbol{k}_s)sgn(\dot{\boldsymbol{q}})$, where $\boldsymbol{k}_v$, $\boldsymbol{k}_s \in R^{n\times 1}$ are constant friction coefficients. Let $\bar{\boldsymbol{k}}_v, \bar{\boldsymbol{k}}_s \in R^{n\times 1}$ be the estimated friction coefficients. Then, $\boldsymbol{\tau}_f - \bar{\boldsymbol{\tau}}_f - \boldsymbol{Y}\widetilde{\boldsymbol{\phi}}$ can be written as $-\boldsymbol{Y}_E\widetilde{\boldsymbol{\phi}}_E$, where $\boldsymbol{Y}_E = [\boldsymbol{Y}, diag(\dot{\boldsymbol{q}}), diag(sgn(\dot{\boldsymbol{q}}))]$; $\widetilde{\boldsymbol{\phi}}_E = \bar{\boldsymbol{\phi}}_E - \boldsymbol{\phi}_E$; $\bar{\boldsymbol{\phi}}_E$ is $[\bar{\boldsymbol{\phi}}^T, \bar{\boldsymbol{k}}_v^T, \bar{\boldsymbol{k}}_s^T]^T$; $\boldsymbol{\phi}_E$ is $[\boldsymbol{\phi}^T, \boldsymbol{k}_v^T, \boldsymbol{k}_s^T]^T$.

Let the Cartesian position and the rotation matrix satisfying (4) be the reference Cartesian position $\boldsymbol{p}_r$ and the reference rotation matrix $\boldsymbol{R}_r$, i.e., there is $\boldsymbol{R}_r = e^{(\theta\boldsymbol{l})_r}\boldsymbol{R}_d$ referring to (5), and $\boldsymbol{p}_r$ and $(\theta\boldsymbol{l})_r$ satisfy

$$\boldsymbol{M}\begin{bmatrix}\ddot{\boldsymbol{p}}_r - \ddot{\boldsymbol{p}}_d \\ (\dot{\theta\boldsymbol{l}})_r\end{bmatrix} + \boldsymbol{D}\begin{bmatrix}\dot{\boldsymbol{p}}_r - \dot{\boldsymbol{p}}_d \\ (\dot{\theta\boldsymbol{l}})_r\end{bmatrix} + \boldsymbol{K}\begin{bmatrix}\boldsymbol{p}_r - \boldsymbol{p}_d \\ (\theta\boldsymbol{l})_r\end{bmatrix} = \begin{bmatrix}\boldsymbol{f}_e - \boldsymbol{f}_d \\ \boldsymbol{\tau}_e - \boldsymbol{\tau}_d\end{bmatrix} \tag{18}$$

The values of $\boldsymbol{p}_r$, $(\theta\boldsymbol{l})_r$, and $\boldsymbol{R}_r$, along with their derivatives, can be obtained by solving the above differential equation after measuring the external effort. By subtracting (17) from (18), and denoting $\left[\boldsymbol{p}^T - \boldsymbol{p}_r^T, (\theta\boldsymbol{l})^T - (\theta\boldsymbol{l})_r^T\right]^T$ as $\boldsymbol{e}$, it has

$$-\boldsymbol{M}\boldsymbol{J}'\bar{\boldsymbol{B}}^{-1}\boldsymbol{Y}_E\widetilde{\boldsymbol{\phi}}_E + \boldsymbol{M}\ddot{\boldsymbol{e}} + \boldsymbol{D}\dot{\boldsymbol{e}} + \boldsymbol{K}\boldsymbol{e} = \boldsymbol{0} \tag{19}$$

Following the steps in [11], the adaptation of estimated dynamic parameters could be

$$\dot{\widetilde{\boldsymbol{\phi}}}_E = -\boldsymbol{\Psi}\boldsymbol{Y}_E^T\bar{\boldsymbol{B}}^{-T}\boldsymbol{J}'^T(\dot{\boldsymbol{e}} + \boldsymbol{\Phi}\boldsymbol{e}) \tag{20}$$

where $\boldsymbol{\Psi} \in R^{13n\times 13n}$ is a proper positive definite matrix, and $\boldsymbol{\Phi} \in R^{n\times n}$ could be a diagonal positive definite matrix. Additionally, according to [11], an extra term can be added to the command torque to handle measurement noise without affecting the form of the adaptation law (20). According to [11], with the above adaptation law, $\boldsymbol{e}$ converges to $\boldsymbol{0}$, i.e., $\boldsymbol{p}$ converges to $\boldsymbol{p}_r$ and $\boldsymbol{R}$ converges to $\boldsymbol{R}_r$. Since $\boldsymbol{p}_r$ and $\boldsymbol{R}_r$ satisfy (4), with the help of the adaptation law (20), the actual $\boldsymbol{p}$ and $\boldsymbol{R}$ would also satisfy (4), i.e., the desired dynamic relationship can be realized accurately.

The adaptive control here belongs to the kind of direct adaptive control, and the estimation of the dynamic parameters will not converge to the true values. While, when only achieving the desired impedance model is required, it is not necessary for the estimated parameters to converge to the true parameters. Both the theory presented here and the subsequent experiments demonstrate that the lack of parametric convergence does not prevent achieving the desired impedance model.

According to (19), some other conclusions can also be drawn when only (16) is used without the adaptation law (20). Since (4) is a second-order linear system, $\boldsymbol{M}$, $\boldsymbol{D}$, and $\boldsymbol{K}$ can be chosen easily such that (4) is an asymptotically stable system. For (19), with these impedance parameters, the second-order system $\boldsymbol{M}\ddot{\boldsymbol{e}} + \boldsymbol{D}\dot{\boldsymbol{e}} + \boldsymbol{K}\boldsymbol{e} = \boldsymbol{0}$ is also an asymptotically stable system. According to the input-output stability theory, it's easy to know that $\dot{\boldsymbol{e}}$ and $\boldsymbol{e}$ are bounded when $\widetilde{\boldsymbol{\phi}}_E$ is small and the first term of (19) is bounded. Furthermore, in this situation, $\boldsymbol{p}$ and $\boldsymbol{R}$ are in the neighborhoods of $\boldsymbol{p}_r$ and $\boldsymbol{R}_r$, and $\dot{\boldsymbol{p}}$ and $\dot{\boldsymbol{R}}$ are in the neighborhoods of $\dot{\boldsymbol{p}}_r$ and $\dot{\boldsymbol{R}}_r$.

IV. Simulation

A simulation is conducted to illustrate the difference between the two impedance models (3) and (4). In this simulation, it is assumed that both (3) and (4) can be accurately achieved. Since only the high-order terms in the rotation-torque part of the impedance model have been modified, only the rotation-torque part is considered here. Therefore, in Fig. 1(a) and (b), only orientation and rotation are taken into account, and let's ignore the position of objects in those figures.

As shown in Fig. 1(a), suppose $\boldsymbol{R}_d$ is stable and equals to $\boldsymbol{I}$; let $\boldsymbol{R} = \boldsymbol{I}$ and $\ddot{\boldsymbol{R}} = \dot{\boldsymbol{R}} = \boldsymbol{0}$ at 0 s. Assume that $\boldsymbol{M}$, $\boldsymbol{D}$, $\boldsymbol{K}$, and

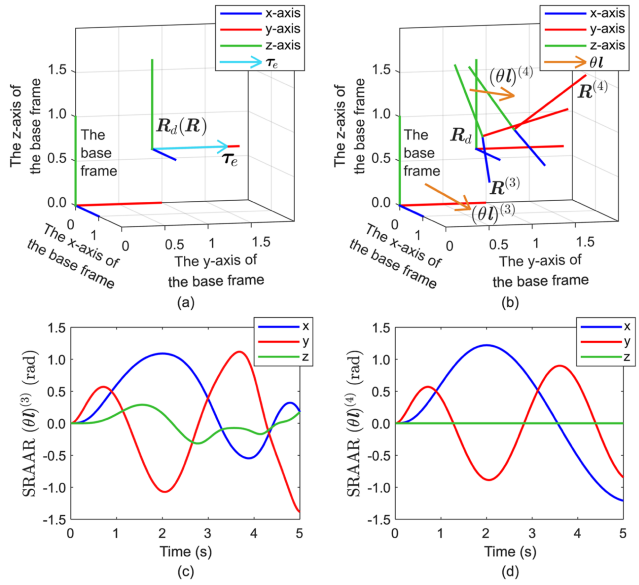

Fig. 1. Simulation figures. (a) Initial $\boldsymbol{R}_d$, $\boldsymbol{R}$, and $\boldsymbol{\tau}_e$ at 0 s. (b) $\boldsymbol{R}_d$, $\boldsymbol{R}^{(3)}$, $\boldsymbol{R}^{(4)}$, $(\theta\boldsymbol{l})^{(3)}$, and $(\theta\boldsymbol{l})^{(4)}$ at 3 s. (c) The value of $(\theta\boldsymbol{l})^{(3)}$ in 5 s. (d) The value of $(\theta\boldsymbol{l})^{(4)}$ in 5 s.

$\boldsymbol{\tau}_d$ in (3) and (4) are $0.1\boldsymbol{I}$, $0.4\boldsymbol{I}$, $\boldsymbol{I}$, and $\boldsymbol{0}$, respectively. Suppose there is a torque $\boldsymbol{\tau}_e$ applied to $\boldsymbol{R}$, and $\boldsymbol{\tau}_e$ is always in the XY plane of the base frame; let $\boldsymbol{\tau}_e$ be $\left[1.2sin(t), 0.9cos(2t), 0\right]^T$. Then, $\boldsymbol{R}$ will start rotating under the influence of $\boldsymbol{\tau}_e$.

Fig. 1(b) shows the different $\boldsymbol{R}$ corresponding to (3) and (4) at 3 s, and it uses $\boldsymbol{R}^{(3)}$ and $\boldsymbol{R}^{(4)}$ to distinguish between them. The orange lines represent the vectors of SRAAR of $\boldsymbol{R}$ and are distinguished by $(\theta\boldsymbol{l})^{(3)}$ and $(\theta\boldsymbol{l})^{(4)}$. Fig. 1(c) and (d) display the values of $(\theta\boldsymbol{l})^{(3)}$ and $(\theta\boldsymbol{l})^{(4)}$ from 0 s to 5 s. It can be observed that the third component of $(\theta\boldsymbol{l})^{(4)}$ is always 0, which means the rotation axis between $\boldsymbol{R}_d$ and $\boldsymbol{R}$ also always lies in the XY plane of the base frame. Therefore, one dimension in the rotation-torque part of (4) could be ignored, whereas, no such characteristic exists for $(\theta\boldsymbol{l})^{(3)}$.

It should be pointed out that, although all vectors in (4) are defined in the base frame, these vectors can be represented in different coordinates through rotation transformations according to the application's needs. Then, the modified (4) can be obtained. Following the steps in the former sections, all the above equations and characteristics have corresponding versions. For example, let's use $\boldsymbol{R}^T(\theta\boldsymbol{l})(=\boldsymbol{R}_d^T(\theta\boldsymbol{l}))$ and $\boldsymbol{R}^T(\boldsymbol{\tau}_e - \boldsymbol{\tau}_d)$ to replace $(\theta\boldsymbol{l})$ and $\boldsymbol{\tau}_e - \boldsymbol{\tau}_d$ in (4). The modified (4) can be used in applications where a flat surface and a convex surface are in contact. The characteristic mentioned in the previous paragraph can be exploited to simplify the analysis when the orientation or torque of the end-effector needs to be controlled.

V. Experiment

Based on the proposed SRAAR-based second-order impedance control, an adaptive algorithm is proposed to eliminate the effects of dynamic parameter errors so that the desired impedance model can be realized accurately. The effectiveness of the adaptive algorithm signifies the correctness of the proposed second-order impedance control and also embodies the

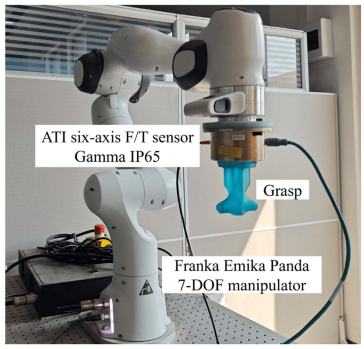

Fig. 2. The system setup.

significance of the second-order impedance control. Thus, in the following, it uses the torque obtained by (16) without the adaptation law (20) and the torque obtained by (16) with the adaptation law (20) to control the manipulator, respectively.

A. System Setup

The overview of the hardware configuration is shown in Fig. 2. A 7-DOF manipulator, Franka Emika Panda, controlled in torque mode at 1 KHz, is used in the following experiments. An ATI six-axis F/T sensor, Gamma IP65, is used to measure the environment effort applied to the end-effector. Additionally, a grasp is designed for the purpose of making it easier for people to apply effort to the manipulator.

Similar to the approach described in [18], a standard dynamic parameter identification process is implemented to obtain the dynamic parameters of the used manipulator equipped with the ATI sensor.

In the following two experiments, the desired motion in impedance control is set as below. The initial joint position $\boldsymbol{q}_0$ is set to be $\left[0, -\pi/4, 0, -3\pi/4, 0, \pi/2, \pi/4\right]^T$. And at this moment, denote the Cartesian position and the rotation matrix of the end-effector as $\boldsymbol{p}_0$ and $\boldsymbol{R}_0$. $\boldsymbol{p}_d(t)$ is set as $\boldsymbol{p}_0 + \lambda(t)\Delta\boldsymbol{p}_d(t)$ when $t \leq 5\,\mathrm{s}$, and is set as $\boldsymbol{p}_0 + \Delta\boldsymbol{p}_d(t)$ when $t > 5\,s$, where $\lambda(t) = 0.00192t^5 - 0.024t^4 + 0.08t^3$, and λ will go from 0 to 1 smoothly when t goes from 0 s to 5 s. $\boldsymbol{R}_d(t)$ is set as $e^{\theta_{\exp}\boldsymbol{l}_{\exp}/\|\boldsymbol{l}_{\exp}\|}\boldsymbol{R}_0$. In the first experiment, $\theta_{\exp}(t)$, $\boldsymbol{l}_{\exp}$, and $\Delta\boldsymbol{p}_d(t)$ are

$$\begin{cases} \theta_{\exp}(t) = 0.7\sin(0.6\pi t) \\ \boldsymbol{l}_{\exp}(t) = \left[\sin(2t), 1.5\cos(2t), -\cos(t)\right]^T \\ \Delta\boldsymbol{p}_d(t) = \left[0.1\sin(1.5t), 0.15\cos(1.5t), 0.05\sin(2t)\right]^T \end{cases}$$

While, in the second experiment, there is

$$\begin{cases} \theta_{\exp}(t) = 0.6\sin(0.5\pi t) \\ \boldsymbol{l}_{\exp}(t) = \left[\cos(t), 1.5\sin(t), -\cos(2t)\right]^T \\ \Delta\boldsymbol{p}_d(t) = \left[0.1\cos(2t), 0.1\sin(2t), 0.05\sin(3t)\right]^T \end{cases}$$

In (4), $\boldsymbol{M}$ is chosen as $diag(2, 2, 2, 0.05, 0.05, 0.05)$; $\boldsymbol{D}$ is set as $diag(50, 50, 50, 1.25, 1.25, 1.25)$; $\boldsymbol{K}$ is set as $diag(400, 400, 400, 5, 5, 5)$. Besides, $\boldsymbol{f}_d$ and $\boldsymbol{\tau}_d$ are set as $\boldsymbol{0}$. And in (20), $\boldsymbol{\Psi}$ is $0.01\boldsymbol{I}$, and $\boldsymbol{\Phi} = 50diag(30, 30, 30, 1, 1, 1)$.

It uses $\boldsymbol{\tau} = \boldsymbol{J}'^T\boldsymbol{\eta} + \boldsymbol{N}\boldsymbol{\xi}$ to solve for $\boldsymbol{\tau}$ in (16). $\boldsymbol{\eta}$ can be obtained by multiplying $\boldsymbol{M}\boldsymbol{J}'\bar{\boldsymbol{B}}^{-1}\boldsymbol{J}'^T$ to both sides of (16), and $\boldsymbol{N} = (\boldsymbol{I} - (\boldsymbol{J}'\bar{\boldsymbol{B}}^{-1})^{\dagger}\boldsymbol{J}'\bar{\boldsymbol{B}}^{-1})$, and $\boldsymbol{\xi}$ is $-\boldsymbol{D}_N\dot{\boldsymbol{q}} - \boldsymbol{K}_N(\boldsymbol{q} - \boldsymbol{q}_0)$ where $\boldsymbol{D}_N$ and $\boldsymbol{K}_N$ are set as $10\boldsymbol{I}$. According to [11], an extra term of $-0.6sgn(\bar{\boldsymbol{B}}^{-T}\boldsymbol{J}'^T(\dot{\boldsymbol{e}} + \boldsymbol{\Phi}\boldsymbol{e}))$ is also added to the command torque when the adaptation law is used.

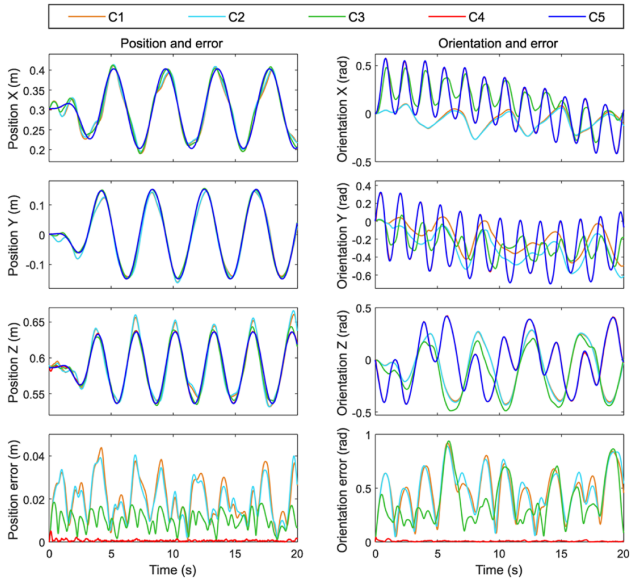

Fig. 3. Motion of the end-effector for C1-C5 when there is no external effort.

B. Impedance Control Without External Effort

In this experiment, the manipulator is required to move under the impedance control without external effort. The actual and the desired motions should be the same.

To make the experimental results more convincing, the dynamic matrices of both the manipulator's own and an open-source dynamic library [18] are also utilized in this experiment. Moreover, no F/T sensor or grasp is employed when these two sets of dynamic parameters are used. Thus, there are four situations. C1: Franka Emika's built-in dynamic parameters, no F/T sensor, grasp, or adaptive algorithm. C2: Open-source dynamic parameters [18], no F/T sensor, grasp, or adaptive algorithm. C3: Identified dynamic parameters, with F/T sensor and grasp but no adaptive algorithm. C4: Identified dynamic parameters, with F/T sensor, grasp, and adaptive algorithm. Besides, the desired motion is represented as C5.

The experimental results are shown in Fig. 3. The figures in the left column of Fig. 3, from top to bottom, show the Cartesian positions in the X, Y, and Z directions, and show the Cartesian position error between the actual position and the desired position from C1 to C5. The position error is the Cartesian distance directly. If we use $(\theta\boldsymbol{l})^{\overrightarrow{R_aR_b}}$ to represent the SRAAR between rotation matrices $\boldsymbol{R}_a$ and $\boldsymbol{R}_b$, i.e., $\boldsymbol{R}_b = exp((\theta\boldsymbol{l})^{\overrightarrow{R_aR_b}})\boldsymbol{R}_a$ referring to (5), the figures in the right column of Fig. 3, from top to bottom, show the three components of the orientation represented by SRAAR, and show the orientation error, under cases C1 to C5. For C1 to C4, the orientations X, Y, and Z in Fig. 3 are the three components of $(\theta\boldsymbol{l})^{\overrightarrow{R_0R}}$, and the orientation error is the norm of $(\theta\boldsymbol{l})^{\overrightarrow{R_dR}}$. For C5, the orientations X, Y, and Z are the three components of $(\theta\boldsymbol{l})^{\overrightarrow{R_0R_d}}$.

In Fig. 3, for the position tracking problem, C1 (Franka Emika's built-in dynamic parameters) and C2 (the open-source dynamic parameters) have a similar effect and are obviously worse than C3 (the identified dynamic parameters). And for the orientation tracking problem, as shown in Fig. 3, C1 to C3 have similar results, and there is a big gap between the curves of these three cases and the curve of C5. However, obviously, C4 has the best tracking effect for both position tracking and orientation tracking. The curve of C4 almost coincides with the curve of C5, which is completely different from the previous three cases, which means the impedance model is realized accurately in this situation. For C1 to C4, the average position errors are 20.536 mm, 19.679 mm, 10.135 mm, and 0.627 mm, respectively, and the average orientation errors are 0.4764 rd, 0.4824 rd, 0.3786 rd, and 0.0072 rd, respectively.

Two conclusions can be drawn from this experiment, one is the proposed adaptive algorithm is effective in this case, and the other one is that the dynamic parameters identified by ourselves result in better performance on our robot. The first conclusion is the premise for studying the situation where environmental effort exists, and utilizing the second conclusion, only the identified dynamic parameters will be considered in the following experiment.

C. Impedance Control With External Effort

In this experiment, the manipulator is also required to move under the impedance control, and there would be a random external effort applied by a human to the end-effector. The actual and the desired motions should satisfy (4). The difference between $\boldsymbol{R}_r$, $\boldsymbol{p}_r$ and $\boldsymbol{R}$, $\boldsymbol{p}$ reflects whether the actual movement satisfies the given desired impedance model.

When the manipulator starts moving, there will be no effort in the first 4 seconds. Then, a random effort will be applied by a human to the end-effector in the next 12 seconds. In the last 4 seconds, the force will be removed.

The results are shown in Fig. 4 and Fig. 5. The blue line represents the value of desired motion; the value of reference motion is represented by the green line; the value of actual motion is represented by the red line. The figures in the left column of Fig. 4 and Fig. 5, from top to bottom, show the external forces; show the actual, desired, and reference Cartesian positions in the X, Y, and Z directions; show the Cartesian position error between the actual position and the reference position. The external forces and Cartesian positions are expressed under the base frame, and the position error is the Cartesian distance directly. The figures in the right column of Figs. 4 and 5, from top to bottom, show the external torques expressed under the base frame; show the three components of the orientation represented by SRAAR under $\boldsymbol{R}_0$, i.e., the three components of $(\theta\boldsymbol{l})^{\overrightarrow{R_0R_d}}$, $(\theta\boldsymbol{l})^{\overrightarrow{R_0R_r}}$, or $(\theta\boldsymbol{l})^{\overrightarrow{R_0R}}$; and show the orientation error between $\boldsymbol{R}$ and $\boldsymbol{R}_r$, i.e., the norm of $(\theta\boldsymbol{l})^{\overrightarrow{R_rR}}$.

It can be observed from Fig. 4 that there is always a relatively large position error and orientation error between the actual motion and the reference motion. However, those errors are much smaller for C4 from beginning to end, which means that the desired impedance model is realized accurately all the time. For C3, the average position error is 9.810 mm, and the average orientation error is 0.3444 rd. For C4, the average position error is 0.702 mm, and the average orientation error is 0.0054 rd, significantly smaller than the errors of C3, which verifies the effectiveness of the proposed adaptive algorithm.

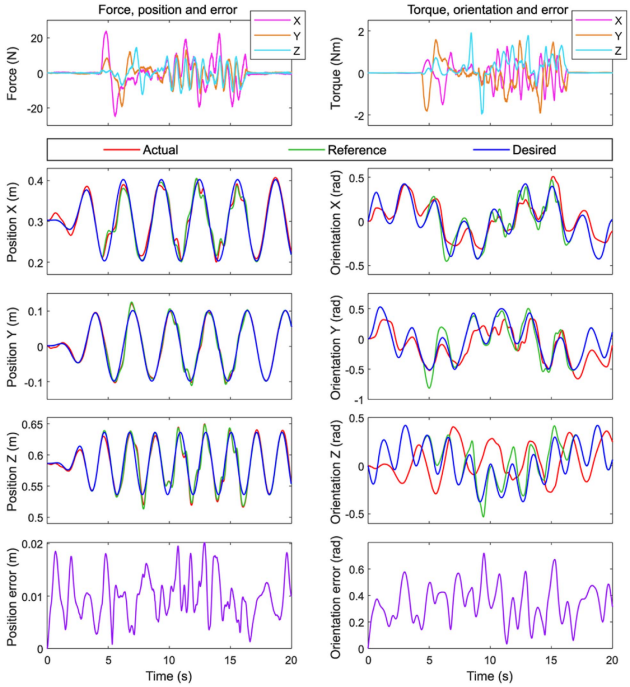

Fig. 4. Environmental effort and end-effector motion for C3.

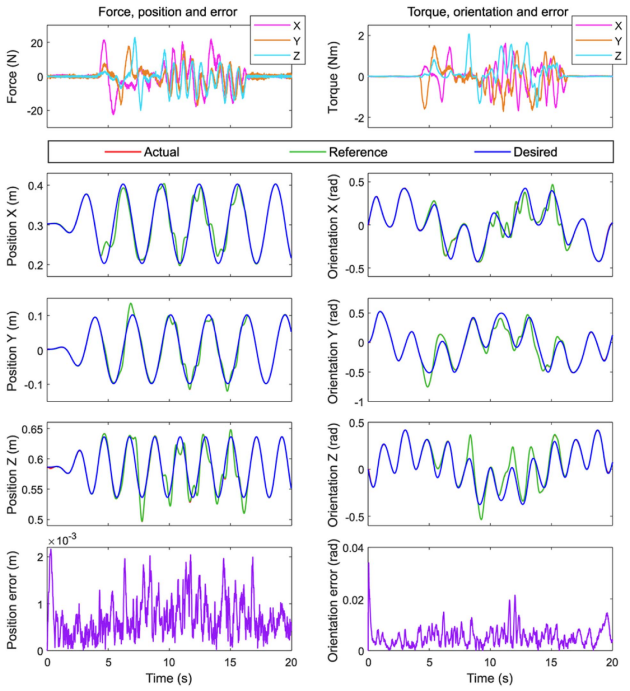

Fig. 5. Environmental effort and end-effector motion for C4.

It should be emphasized again that the proposed adaptive algorithm requires the impedance model to have the form of SODE and is a direct application result of the proposed SRAAR-based second-order impedance control. Therefore, the effectiveness of

the proposed adaptive algorithm also demonstrates the application potential and the advantages of the proposed second-order impedance model.

VI. Conclusion

This letter employs simple-rotation angle/axis representations together with their derivatives to describe the end-effector's orientation displacement and its derivatives in impedance control. A method for obtaining the first derivative of SRAAR is provided, utilizing two auxiliary variables to simplify the calculation. Subsequently, complete first-order and second-order differential relationships between SRAAR and joint angles are also proposed. Then, a type of SRAAR-based second-order impedance control, which has the form of SODE, is realized. Finally, based on the proposed second-order impedance control, a novel kind of adaptive control is also proposed. This adaptive control is a direct application result of the proposed SRAAR-based second-order impedance control and demonstrates the application potential and the advantages of the proposed second-order impedance model. Simulation shows that, even with the same external effort, the classical impedance control and the proposed impedance control may have different dynamic characteristics. Two experiments validate the effectiveness of the proposed adaptive control, which also shows the correctness of the proposed SRAAR-based second-order impedance control.

Appendix
Differential relationship between $\theta\boldsymbol{l}$ and $\boldsymbol{q}$ when $\theta = 0$

When $\theta = 0$, it has $\dot{\tilde{\boldsymbol{R}}} = \dot{\theta}\hat{\boldsymbol{l}} = \widehat{(\dot{\theta}\boldsymbol{l})}$. Because $(\dot{\theta}\boldsymbol{l})$ is a 3D vector, $(\dot{\theta}\boldsymbol{l})$ can always be a linear combination of three orthonormal bases. Suppose $\boldsymbol{v}_1, \boldsymbol{v}_2, \boldsymbol{v}_3$ are the three orthonormal bases satisfying $\boldsymbol{v}_1 \times \boldsymbol{v}_2 = \boldsymbol{v}_3$, and let $\boldsymbol{v}_4 = \boldsymbol{v}_1$ and $\boldsymbol{v}_5 = \boldsymbol{v}_2$. Then, there always exist x_1, x_2, and x_3 such that $(\dot{\theta}\boldsymbol{l}) = x_1\boldsymbol{v}_1 + x_2\boldsymbol{v}_2 + x_3\boldsymbol{v}_3$. Multiply $\boldsymbol{v}_2^T$ left by $\dot{\tilde{\boldsymbol{R}}}$ and then multiply $\boldsymbol{v}_1$ right by $\dot{\tilde{\boldsymbol{R}}}$; it yields $x_3 = \boldsymbol{v}_2^T\dot{\tilde{\boldsymbol{R}}}\boldsymbol{v}_1$. Similarly, it yields $x_1 = \boldsymbol{v}_3^T\dot{\tilde{\boldsymbol{R}}}\boldsymbol{v}_2$ and $x_2 = \boldsymbol{v}_1^T\dot{\tilde{\boldsymbol{R}}}\boldsymbol{v}_3$. Using $\dot{\boldsymbol{R}} = \widehat{\boldsymbol{J}_o\dot{\boldsymbol{q}}}\boldsymbol{R}$, $(\dot{\theta}\boldsymbol{l}) = \boldsymbol{v}_1x_1 + \boldsymbol{v}_2x_2 + \boldsymbol{v}_3x_3$ can be reshaped as $(\dot{\theta}\boldsymbol{l}) = \boldsymbol{J}_{o_3'}\dot{\boldsymbol{q}} + \boldsymbol{\gamma}_3$, where

$$\boldsymbol{J}_{o_3'} = -\sum_{i=1}^{3}\boldsymbol{v}_i\boldsymbol{v}_{i+2}^T(\widehat{\boldsymbol{R}\boldsymbol{R}_d^T\boldsymbol{v}_{i+1}})\boldsymbol{J}_o \tag{21}$$

$$\boldsymbol{\gamma}_3 = \sum_{i=1}^{3}\boldsymbol{v}_i\boldsymbol{v}_{i+2}^T\boldsymbol{R}\dot{\boldsymbol{R}}_d^T\boldsymbol{v}_{i+1} \tag{22}$$

When $\theta = 0$, it has $\ddot{\tilde{\boldsymbol{R}}} = \dot{\theta}\hat{\boldsymbol{l}}$ and $\dddot{\tilde{\boldsymbol{R}}} = \dot{\theta}^2\hat{\boldsymbol{l}}\hat{\boldsymbol{l}} + \ddot{\theta}\hat{\boldsymbol{l}} + 2\dot{\theta}\dot{\hat{\boldsymbol{l}}}$. Thus, there is $\dddot{\tilde{\boldsymbol{R}}} = \ddot{\tilde{\boldsymbol{R}}}\dot{\tilde{\boldsymbol{R}}} + \hat{\boldsymbol{\xi}}$, where $\boldsymbol{\xi} = \ddot{\boldsymbol{\theta}}\boldsymbol{l} + 2\dot{\theta}\dot{\boldsymbol{l}} = (\ddot{\theta}\boldsymbol{l})$. Because $\boldsymbol{\xi}$ is a 3D vector, similar to before, $\boldsymbol{\xi}$ can always be a linear combination of three orthonormal bases, i.e., $\boldsymbol{\xi} = x_1'\boldsymbol{v}_1 + x_2'\boldsymbol{v}_2 + x_3'\boldsymbol{v}_3$. Multiply $\boldsymbol{v}_2^T$ left by $\dddot{\tilde{\boldsymbol{R}}}$ and then multiply $\boldsymbol{v}_1$ right by $\dddot{\tilde{\boldsymbol{R}}}$; it yields $x_3' = \boldsymbol{v}_2^T\dddot{\tilde{\boldsymbol{R}}}\boldsymbol{v}_1 - \boldsymbol{v}_2^T\ddot{\tilde{\boldsymbol{R}}}\dot{\tilde{\boldsymbol{R}}}\boldsymbol{v}_1$. Similarly, it yields $x_1' = \boldsymbol{v}_3^T\dddot{\tilde{\boldsymbol{R}}}\boldsymbol{v}_2 - \boldsymbol{v}_3^T\ddot{\tilde{\boldsymbol{R}}}\dot{\tilde{\boldsymbol{R}}}\boldsymbol{v}_2$ and $x_2' = \boldsymbol{v}_1^T\dddot{\tilde{\boldsymbol{R}}}\boldsymbol{v}_3 - \boldsymbol{v}_1^T\ddot{\tilde{\boldsymbol{R}}}\dot{\tilde{\boldsymbol{R}}}\boldsymbol{v}_3$. Using $\ddot{\boldsymbol{R}} = \widehat{(\dot{\boldsymbol{J}}_o\dot{\boldsymbol{q}} + \boldsymbol{J}_o\ddot{\boldsymbol{q}})}\boldsymbol{R} + \widehat{\boldsymbol{J}_o\dot{\boldsymbol{q}}}\widehat{\boldsymbol{J}_o\dot{\boldsymbol{q}}}\boldsymbol{R}$, $(\ddot{\theta}\boldsymbol{l}) = \boldsymbol{v}_1x_1' + \boldsymbol{v}_2x_2' + \boldsymbol{v}_3x_3'$ can be reshaped as $(\ddot{\theta}\boldsymbol{l}) = \boldsymbol{J}_{o_3'}\ddot{\boldsymbol{q}} + \boldsymbol{\Gamma}_3$, where $\boldsymbol{J}_{o_3'}$ is just the same as (21), and $\boldsymbol{\Gamma}_3$ is

$$\begin{aligned}\boldsymbol{\Gamma}_3 = &-\sum_{i=1}^{3}\boldsymbol{v}_i\boldsymbol{v}_{i+2}^T(\widehat{\boldsymbol{R}\boldsymbol{R}_d^T\boldsymbol{v}_{i+1}})\dot{\boldsymbol{J}}_o\dot{\boldsymbol{q}} + \sum_{i=1}^{3}\boldsymbol{v}_i\boldsymbol{v}_{i+2}^T(-\ddot{\tilde{\boldsymbol{R}}}\dot{\tilde{\boldsymbol{R}}}\\ &+\widehat{\boldsymbol{J}_o\dot{\boldsymbol{q}}}\widehat{\boldsymbol{J}_o\dot{\boldsymbol{q}}}\boldsymbol{R}\boldsymbol{R}_d^T + 2\dot{\boldsymbol{R}}\dot{\boldsymbol{R}}_d^T + \boldsymbol{R}\ddot{\boldsymbol{R}}_d^T)\boldsymbol{v}_{i+1}\end{aligned} \tag{23}$$

References

[1] N. Hogan, "Impedance control: An approach to manipulation," in *Proc. IEEE Amer. Control Conf.*, 1984, pp. 304–313.

[2] F. Caccavale, B. Siciliano, and L. Villani, "The tricept robot: Dynamics and impedance control," *IEEE/ASME Trans. Mechatron.*, vol. 8, no. 2, pp. 263–268, Jun. 2003.

[3] L. Sciavicco and B. Siciliano, *Modelling and Control of Robot Manipulators*. New York, NY, USA: Springer, 2001.

[4] F. Caccavale, C. Natale, B. Siciliano, and L. Villani, "Six-DoF impedance control based on angle/axis representations," *IEEE Trans. Robot. Automat.*, vol. 15, no. 2, pp. 289–300, Apr. 1999.

[5] G. Ferretti, G. Magnani, and P. Rocco, "Impedance control for elastic joints industrial manipulators," *IEEE Trans. Robot. Automat.*, vol. 20, no. 3, pp. 488–498, Jun. 2004.

[6] J. Jeong, H. Mishra, C. Ott, and M. J. Kim, "A memory-based SO(3) parameterization: Theory and application to 6D impedance control with radially unbounded potential function," in *Proc. IEEE Int. Conf. Robot. Automat.*, 2022, pp. 8338–8344.

[7] J. L. Crassidis and F. L. Markley, "Sliding mode control using modified rodrigues parameters," *J. Guid., Control, Dyn.*, vol. 19, no. 6, pp. 1381–1383, 1996.

[8] R. Volpe and P. Khosla, "The equivalence of second-order impedance control and proportional gain explicit force control," *Int. J. Robot. Res.*, vol. 14, no. 6, pp. 574–589, 1995.

[9] F. Caccavale, P. Chiacchio, A. Marino, and L. Villani, "Six-DoF impedance control of dual-arm cooperative manipulators," *IEEE/ASME Trans. On Mechatron.*, vol. 13, no. 5, pp. 576–586, Oct. 2008.

[10] C. Ott, *Cartesian Impedance Control of Redundant and Flexible-Joint Robots*. Ne York, NY, USA: Springer, 2008.

[11] W.-S. Lu and Q.-H. Meng, "Impedance control with adaptation for robotic manipulations," *IEEE Trans. Robot. Automat.*, vol. 7, no. 3, pp. 408–415, Jun. 1991.

[12] S. Jung, T. C. Hsia, and R. G. Bonitz, "Force tracking impedance control of robot manipulators under unknown environment," *IEEE Trans. Control Syst. Technol.*, vol. 12, no. 3, pp. 474–483, May 2004.

[13] J. Duan, Y. Gan, M. Chen, and X. Dai, "Adaptive variable impedance control for dynamic contact force tracking in uncertain environment," *Robot. Auton. Syst.*, vol. 102, pp. 54–65, 2018.

[14] K. Kronander and A. Billard, "Stability considerations for variable impedance control," *IEEE Trans. Robot.*, vol. 32, no. 5, pp. 1298–1305, Oct. 2016.

[15] F. Bullo and R. M. Murray, "Proportional derivative (PD) control on the Euclidean group," in *Proc. Eur. Control Conf.*, 1995, pp. 1091–1097.

[16] R. Campa and H. De La Torre, "Pose control of robot manipulators using different orientation representations: A comparative review," in *Proc. IEEE Amer. Control Conf.*, 2009, pp. 2855–2860.

[17] H. Wang, "Adaptive control of robot manipulators with uncertain kinematics and dynamics," *IEEE Trans. Autom. Control*, vol. 62, no. 2, pp. 948–954, Feb. 2017.

[18] C. Gaz, M. Cognetti, A. Oliva, P. R. Giordano, and A. De Luca, "Dynamic identification of the Franka Emika panda robot with retrieval of feasible parameters using penalty-based optimization," *IEEE Robot. Automat. Lett.*, vol. 4, no. 4, pp. 4147–4154, Oct. 2019.